

Is the HEFT matching unique?

Sally Dawson^{*1}, Duarte Fontes^{†1}, Carlos Quezada-Calonge^{‡2}, and Juan José Sanz-Cillero^{§2}

¹*Department of Physics, Brookhaven National Laboratory, Upton, New York 11973 U.S.A.*

²*Departamento de Física Teórica and IPARCOS, Universidad Complutense de Madrid,
Plaza de las Ciencias 1, 28040-Madrid, Spain*

Physics beyond the Standard Model (BSM) can be described in a consistent and general way through the Higgs Effective Field Theory (HEFT). Measurements of model-independent HEFT coefficients allow one to constrain the parameter space of BSM models via a matching procedure. In this work, we show that this procedure is not unique and depends on the scalings of the parameters of the Lagrangian. As examples, we consider three BSM models: the real singlet extension of the SM with a Z_2 symmetry, the complex singlet extension (CSE) of the SM and the 2 Higgs Doublet Model. We discuss several physical observables, and show that different scalings of the model parameters with the UV scale in the matching to the HEFT can yield quite different results. This complicates the interpretation of HEFT measurements in terms of parameters of BSM models. Additionally, as a by-product, we report the first matching of the CSE to the HEFT.

1 Introduction

The discovery of a scalar particle at the Large Hadron Collider (LHC) in 2012 [1, 2] — usually identified as the last piece of the Standard Model (SM), the Higgs boson — intensified an old question: is there physics beyond the SM (BSM)? The absence of any detection of new physics at the LHC suggests that potential BSM physics should be heavy. In that case, the general and consistent framework of an Effective Field Theory (EFT) is ideal to parametrize possible deviations of the SM at the LHC. The two main EFTs for physics that could affect the Higgs sector are the Standard Model EFT (SMEFT) [3–5] and the Higgs EFT (HEFT) [6–13]; for an introduction to both and to their comparison, see refs. [14, 15].

Any EFT is constructed on the basis of an expansion; the set of rules that organizes the order of such expansion — by determining how the different quantities scale — is known as *power counting* (PC). Between the SMEFT and the HEFT, the former is more widely used given its clear PC [14]. Indeed, the SMEFT is the default choice in many LHC analyses and allows for the inclusion of data from many different processes (Higgs physics, di-boson production, electroweak precision measurements and top quark physics, among others) [16–18]. On the other hand, the HEFT is more general than the SMEFT, and has been the object of diverse studies in recent years [19–44], extending previous LHC analyses of leading and subleading HEFT couplings [13, 45–53]. The larger freedom provided by the HEFT has also recently motivated the ATLAS collaboration at the LHC to perform an analysis utilizing the HEFT, in

^{*}dawson@bnl.gov

[†]dfontes@bnl.gov

[‡]cquezada@ucm.es

[§]jj sanz cillero@ucm.es

the context of double Higgs production [54]. This suggests that future experimental analyses related to the exploration of Higgs self-interactions may also find the HEFT parametrization useful.

However, the HEFT is a weak scale effective description of some complete ultraviolet (UV) model. Ultimately, then, one will need to convert the HEFT parametrization to that of a particular UV model. The procedure that allows one to relate the EFT to some higher-energy theory is known as *matching*. Matching is essential both in the scenario where non-zero HEFT coefficients are observed (in which case one would have found BSM physics, and would seek a UV model that could accommodate it), as well as in the scenario where all HEFT coefficients are consistent with the SM (in which case one uses the constraints of the HEFT coefficients to constrain the parameter space of UV models). The HEFT has often been matched to composite Higgs models [28, 55–59]. Up to our knowledge, in 2016 ref. [60] performed for the first time the matching of the HEFT to a UV complete model, by considering a Z_2 -symmetric real singlet extension (Z2RSE) of the SM. Very recently, the same exercise has been performed in the 2 Higgs Doublet Model (2HDM) [38, 39].

Naively, the matching between the HEFT and a UV model with heavy particles is done simply by performing an expansion in inverse powers of the heavy physical masses. This seems to define an unambiguous expansion, i.e. a unique PC. In this paper, we question this reasoning. We show that the existence of a multiplicity of choices for independent parameters complicates the problem. In fact, even if one adopts an expansion simply in inverse powers of the heavy physical masses, very different PCs are obtained according to the set of parameters taken as independent, as different sets imply different scalings. More interestingly, instead of happening that a single PC is always most adequate for all observables, one should in general use different PCs to ensure a fast replication of the results in the UV model for different processes or different regions of the parameter space. This complicates the interpretation of HEFT measurements in terms of parameters of UV models.¹ We illustrate these features by considering three UV models: the Z2RSE, the complex singlet extension (CSE) of the SM and the 2HDM. For each one, we present three PCs, and study the quality with which they replicate the full model in different observables.

The paper is organized as follows: we start by presenting the models and the PCs in Section 2. In this section, we also discuss how to compare the SMEFT and the HEFT matchings, and we write all matching relations. We then present our results in Section 3, and we summarize our conclusions in Section 4. The Appendix provides extra details about the HEFT approach to the CSE.

2 Models, countings and matchings

In this section, we describe the models discussed in this article. For each case, we provide the Lagrangian, discuss relevant choices of independent parameters and relevant Feynman rules, describe the restrictions to the parameter space of the model, and present the PCs to be investigated. Some introductory notes are in order:

1. In all the three models considered in this paper, we assume that all the particles beyond the SM

¹For details on the low-energy HEFT expansion, see refs. [61–66].

are heavy, so that the SM can represent an EFT of the model at stake.

2. The notion of PC is usually employed in the literature from a bottom-up perspective, where the EFT is not bound to any particular UV completion (for an excellent discussion, see ref. [14]). Here we use the term in a broader sense, to describe any set of rules that fixes the different orders of the EFT expansion. In particular, the notion of PC in that sense characterizes a certain matching between a UV model and the HEFT. Different matchings between the UV model and the HEFT therefore correspond to different PCs.
3. We follow ref. [38] in organizing the PCs via a small auxiliary parameter ξ , corresponding to an inverse heavy scale (see also ref. [67]). More specifically, if $v \sim 250$ GeV represents the electroweak scale and $\Lambda \sim 800$ GeV some heavy scale, we estimate $\xi \sim (v/\Lambda)^2 \sim 0.1$. The effective Lagrangian, being an expansion in inverse powers of the heavy scale, can thus be written as an expansion in non-negative powers of ξ . All PCs discussed in this paper lead to well-defined expansions, in the sense that the effective Lagrangians do not contain negative powers of ξ (i.e. positive powers of the large scale). In a certain model, the different PCs differ in the way they attribute different scalings in powers of ξ to the parameters. In general, the different scalings do not have a specific physical motivation; they are considered solely with the purpose of illustrating different possibilities of matching.
4. It should be clear that we are not performing an exhaustive study; that is, we will not consider all possible PCs that could be considered. Rather, the goal is to illustrate the multiplicity of possible matchings between HEFT and a given UV model, and to discuss relevant features of that multiplicity.
5. We shall present in all models the *decoupling* PC. This is the PC consistent with the decoupling limit of the model at stake. In other words, the decoupling PC is such that, on the one hand, the trivial order (ξ^0) of the effective Lagrangian is the SM Lagrangian and, on the other, the quartic parameters of the potential do not scale with the heavy masses, in accordance with perturbative unitarity (for a recent discussion, see ref. [38]).² Then, for the decoupling PC, the $\mathcal{O}(\xi^1)$ and $\mathcal{O}(\xi^2)$ terms of the effective Lagrangian correspond to the SMEFT dimension-6 and dimension-8 contributions in that model, respectively. Such a coincidence of results has been already observed in the case of the 2HDM in ref. [38]. For simplicity, the decoupling PC of each model will always be represented by the same color (yellow) in all the plots of this paper.
6. For each PC in each model, we provide the matching of the relevant parameters of the HEFT Lagrangian up to $\mathcal{O}(\xi^2)$.

We now turn to the HEFT Lagrangian, which contains an expansion in the number of (covariant) derivatives. At the leading order (LO) in that expansion, the terms of the Lagrangian which will matter for

²In principle, there can be more than one decoupling PC for each model. The investigation of this possibility is beyond the scope of this paper.

the processes discussed in this paper are

$$\mathcal{L}_{\text{HEFT}} \supset \frac{v^2}{4} \mathcal{F}(h) \text{Tr} \{ D_\mu U^\dagger D_\mu U \} + \frac{1}{2} (\partial_\mu h)^2 - V(h), \quad (1)$$

where $v = 246$ GeV is the vacuum expectation value (vev) of the SM Higgs field, D_μ is the covariant derivative, and $\mathcal{F}(h)$ and $V(h)$ are analytical functions, each one consisting of a series in powers of h . In general, one has $D_\mu U = \partial_\mu U + igW_\mu^a \frac{\sigma^a}{2} U - ig'U \frac{\sigma^3}{2} B_\mu$, with $U = 1$ in the particular case of the unitary gauge. In the HEFT, h is a gauge singlet, which allows $\mathcal{F}(h)$ and $V(h)$ to contain arbitrary powers of h :

$$\mathcal{F}(h) = 1 + 2a \frac{h}{v} + b \frac{h^2}{v^2} + \dots, \quad V(h) = \frac{1}{2} m_h^2 h^2 \left(1 + \kappa_3 \frac{h}{v} + \frac{\kappa_4}{4} \frac{h^2}{v^2} + \dots \right), \quad (2)$$

where m_h is the h mass, a , b , κ_3 and κ_4 are arbitrary HEFT couplings, and the dots stand for terms with higher powers of h . These couplings are normalized in such a way that the SM limit is obtained for $a = b = \kappa_3 = \kappa_4 = 1$.

In the case of the 2HDM, we shall also consider the processes $h \rightarrow b\bar{b}$ at tree-level, as well as $h \rightarrow \gamma\gamma$ and $h \rightarrow \gamma Z$ at one-loop (where the existence of a charged Higgs boson has interesting consequences for the EFT). For $h \rightarrow b\bar{b}$, we need to consider the term:

$$\mathcal{L}_{\text{HEFT}} \supset -\mathcal{G}(h) m_b \bar{b}b, \quad (3)$$

where m_b is the b quark mass and $\mathcal{G}(h)$ is another polynomial function of h , such that:

$$\mathcal{G}(h) = 1 + c_1 \frac{h}{v} + \dots, \quad (4)$$

with c_1 another HEFT coupling, with $c_1 = 1$ in the SM. As for $h \rightarrow \gamma\gamma$ and $h \rightarrow \gamma Z$, in order for these processes to be matched to the HEFT, it is necessary to consider the next to leading order (NLO) terms in the derivative expansion of $\mathcal{L}_{\text{HEFT}}$. We follow ref. [39] to write those terms as:

$$\mathcal{L}_{\text{HEFT}} \supset -a_{HBB} \frac{h}{v} \text{Tr} [\hat{B}_{\mu\nu} \hat{B}^{\mu\nu}] - a_{HWW} \frac{h}{v} \text{Tr} [\hat{W}_{\mu\nu} \hat{W}^{\mu\nu}] + a_{H1} \frac{h}{v} \text{Tr} [U \hat{B}_{\mu\nu} U^\dagger \hat{W}^{\mu\nu}], \quad (5)$$

where a_{HBB} , a_{HWW} and a_{H1} are yet other HEFT couplings (which vanish in the SM limit), and:

$$\hat{B}_\mu = g' B_\mu \frac{\sigma^3}{2}, \quad \hat{W}_\mu = g W_\mu^a \frac{\sigma^a}{2}, \quad \hat{B}_{\mu\nu} = \partial_\mu \hat{B}_\nu - \partial_\nu \hat{B}_\mu, \quad \hat{W}_{\mu\nu} = \partial_\mu \hat{W}_\nu - \partial_\nu \hat{W}_\mu + i [\hat{W}_\mu, \hat{W}_\nu]. \quad (6)$$

Then, the relevant couplings for $h \rightarrow \gamma\gamma$ and $h \rightarrow \gamma Z$ are, respectively,

$$a_{h\gamma\gamma} = a_{HBB} + a_{HWW} - a_{H1}, \quad a_{h\gamma Z} = a_{HBB} + a_{HWW} - a_{H1} + \frac{m_Z^2}{2m_W^2} (a_{H1} - 2a_{HBB}). \quad (7)$$

Once the matching to HEFT has been performed, we will express some matching results as $\Delta x = x - 1$, where x represents a generic HEFT coupling. The SM limit is recovered when $\Delta x = 0$. The couplings that we consider in this work are collected in tables 1, 2, 3 and 4.

Finally, a note on the relation between the HEFT and the SMEFT. Since the HEFT is more general than SMEFT, it is always possible to write any SMEFT in HEFT form, but the opposite path is not always guaranteed. It is thus interesting to determine when a given HEFT can be written in SMEFT coordinates. Recently, new approaches have emerged where EFTs are formulated from a geometrical point of view [6, 68–71]. This framework allows to ascertain whether a certain HEFT can be written in

SMEFT coordinates by studying the curvature of the EFT manifold. The gist of the idea is to study the existence of an $O(4)$ fixed point upon which the SMEFT can be formulated. Since the purpose of this paper is to illustrate different matchings in HEFT for multiple UV models, we will not further explore this geometrical interpretation.

2.1 Z2RSE

The model

We start with the simplest extension, Z2RSE. We present here a short review of the model, following ref. [60] (for details, cf. e.g. ref. [72, 73]). The model is obtained by taking the SM (whose Higgs doublet we identify as ϕ) and adding a real singlet S to it, which transforms as $S \rightarrow -S$ under Z_2 . The potential reads:

$$V = -\frac{\mu_1^2}{2}\phi^\dagger\phi - \frac{\mu_2^2}{2}S^2 + \frac{\lambda_1}{4}(\phi^\dagger\phi)^2 + \frac{\lambda_2}{4}S^4 + \frac{\lambda_3}{2}\phi^\dagger\phi S^2, \quad (8)$$

where all the parameters are real. The fields ϕ and S may be parametrized as:

$$\phi = \begin{pmatrix} G^+ \\ \frac{1}{\sqrt{2}}(v + h_1 + iG_0) \end{pmatrix}, \quad S = \frac{v_s + h_2}{\sqrt{2}}, \quad (9)$$

where G^+ and G_0 are respectively the charged and neutral would-be Goldstone bosons, h_1 and h_2 are neutral scalar fields (not yet mass states), and $v = 246$ GeV and v_s are vevs, which we assume to be real without loss of generality. The minimization equations read:

$$\mu_1^2 = \frac{\lambda_1 v^2 + \lambda_3 v_s^2}{2}, \quad \mu_2^2 = \frac{\lambda_3 v^2 + \lambda_2 v_s^2}{2}. \quad (10)$$

The mass states h and H — with masses $m = 125$ GeV and M , respectively — are obtained from h_1 and h_2 by considering a mixing angle χ , such that:

$$\begin{pmatrix} h \\ H \end{pmatrix} = \begin{pmatrix} c_\chi & -s_\chi \\ s_\chi & c_\chi \end{pmatrix} \begin{pmatrix} h_1 \\ h_2 \end{pmatrix}, \quad (11)$$

where we introduced the notation $s_x \equiv \sin x$, $c_x \equiv \cos x$. The model thus contains, besides the SM particles, a heavy real scalar H . One possible set of independent parameters is:

$$v, m, v_s, M, s_\chi. \quad (12)$$

The relations between λ_1 , λ_2 and λ_3 of eq. (8) and the parameters of eq. (12) read:

$$\lambda_1 = \frac{2}{v^2} [M^2 s_\chi^2 - m^2 (s_\chi^2 - 1)] \quad (13a)$$

$$\lambda_2 = \frac{2}{v_s^2} [m^2 s_\chi^2 - M^2 (s_\chi^2 - 1)] \quad (13b)$$

$$\lambda_3 = \frac{2c_\chi s_\chi}{v v_s} (M^2 - m^2). \quad (13c)$$

Another relevant choice uses eq. (10) to replace v_s by μ_2^2 :

$$v, m, \mu_2^2, M, s_\chi. \quad (14)$$

Restrictions

The parameter space of the Z2RSE is restricted by many constraints, both purely theoretical and experimental. Theoretical consistency requires that the scattering amplitudes satisfy perturbative unitarity, that the couplings in the Lagrangian are perturbative, and that the parameters correspond to a minimum of the potential [74, 75]. On the experimental side, the limits come from precision electroweak measurements, including the W boson mass [74, 76], measurements of the Higgs coupling strengths [77], and direct searches for the heavy Higgs boson of the model. Higgs coupling measurements require $|s_\chi| \lesssim 0.3$ for $m \lesssim 2M$. For $M \lesssim 850$ GeV, the most stringent limit comes from the measurement of the W boson mass, while for $M \gtrsim 850$ GeV the strongest limit is from the requirement that the quartic couplings remain perturbative ($\lambda_{1,2,3} < 8\pi$) [78]. The limit from the W boson mass is independent of v_s . Direct searches for the heavy Higgs boson in single H production, as well as searches for the resonant process $pp \rightarrow H \rightarrow hh$, do not significantly change the bounds for M between 600 – 800 GeV [78], which are the typical scales chosen in our plots. We will only consider $|s_\chi| \lesssim 0.2$, which is allowed by all the limits listed here.

Power countings

We consider the following EFT PCs for the Z2RSE:

- PC_1^{R} takes eq. (12) as the set of independent parameters, and imposes the decoupling scaling:

$$M^2 \sim \mathcal{O}(\xi^{-1}), \quad v_s^2 \sim \mathcal{O}(\xi^{-1}), \quad s_\chi^2 \sim \mathcal{O}(\xi). \quad (15)$$

- PC_2^{R} takes eq. (12) as the set of independent parameters, and imposes:

$$M^2 \sim \mathcal{O}(\xi^{-1}). \quad (16)$$

- PC_3^{R} takes eq. (14) as the set of independent parameters, and imposes:

$$M^2 \sim \mathcal{O}(\xi^{-1}). \quad (17)$$

Here and in what follows, any parameter of the chosen set that is not explicitly mentioned is assumed to scale as $\mathcal{O}(\xi^0)$ in that PC. As mentioned above, it is reasonable to use all the three PCs of eqs. 15 to 17 in the matching, as they do not lead to positive powers of M in the effective Lagrangian. PC_1^{R} was put forward at the end of ref. [38] and is the decoupling PC. In fact, and as discussed in ref. [38], eqs. (13a)–(13c) show that the quartic parameters in the UV model do not scale as heavy parameters (i.e. with negative powers of ξ) if the scaling (15) is obeyed. We stress that both the scaling of v_s as a heavy parameter and the scaling of s_χ as a small quantity are crucial to this end. In contrast, by restricting themselves to scaling only M , both PC_2^{R} and PC_3^{R} do lead to negative powers of ξ in the scaling of the quartic parameters. Note that PC_2^{R} is the PC used in ref. [60] in the context of the HEFT. PC_3^{R} is identical to PC_2^{R} , except that it takes μ_2^2 instead of v_s as an independent $\mathcal{O}(\xi^0)$ parameter. We will show that this change has significant consequences. Finally, we checked that, in PC_1^{R} , and for the processes

discussed here, the existence of odd powers of v_s or s_χ does not introduce non-integers powers of ξ in the expansion, as odd powers of v_s always multiply odd powers of s_χ .

The matching results for the different PCs are shown in table 1 up to $\mathcal{O}(\xi^2)$, such that the powers of ξ are explicitly included. It is straightforward to see that all Δx deviations vanish in the alignment limit, $s_\chi = 0$, where the SM couplings are recovered. At LO in ξ , PC_2^{R} yields the results given in ref. [60].

PC	Δa	Δb	$\Delta \kappa_3$	$\Delta \kappa_4$
PC_1^{R}	$-\xi \frac{s_\chi^2}{2}$ $-\xi^2 \frac{s_\chi^4}{8}$	$\frac{-2\xi s_\chi^2}{s_\chi^2 - \frac{2m^2}{M^2}}$ $+\xi^2 s_\chi^2 \left(s_\chi^2 - \frac{2m^2}{M^2} \right)$ $-\frac{v_s s_\chi}{v_s}$	$-\xi \frac{3s_\chi^2}{2} +$ $\xi^2 \frac{s_\chi^3}{8v_s} (3s_\chi v_s - 8v)$	$-\xi \frac{25s_\chi^2}{3} - \xi^2 \frac{s_\chi^2}{3M^2 v_s} \left[28m^2 v_s \right.$ $\left. - M^2 s_\chi (41s_\chi v_s - 38v) \right]$
PC_2^{R}	$c_\chi - 1$	$c_\chi^4 - s_\chi^3 c_\chi \frac{v}{v_s} - 1$ $+\xi \frac{2m^2 s_\chi^2}{M^2 v_s} \left(s_\chi^2 v_s \right.$ $\left. - v_s - c_\chi s_\chi v \right)$	$c_\chi^3 - \frac{s_\chi^3 v}{v_s} - 1$	$-1 - \frac{19c_\chi^2 s_\chi^2 (c_\chi v_s + s_\chi v)^2}{3v_s^2}$ $+\frac{(c_\chi^4 v_s^2 + s_\chi^4 v^2)}{v_s^2}$ $-\xi \frac{28c_\chi^2 m^2 s_\chi^2 (c_\chi v_s + s_\chi v)^2}{3M^2 v_s^2}$ $-\xi^2 \frac{16c^2 m^4 s_\chi^2 (c_\chi v_s + s_\chi v)^2}{3M^4 v_s^2}$
PC_3^{R}	$c_\chi - 1$	$-s_\chi^2 + \xi \frac{s_\chi^2}{M^2} (m^2$ $-\mu_2^2) + \xi^2 \frac{3m^2 s_\chi^2}{M^4}$ $\times (m^2 - \mu_2^2)$	$-1 + c_\chi$ $-\xi \frac{s_\chi^2}{M^2 c_\chi} (m^2 - \mu_2^2)$ $-\xi^2 \frac{m^2 s_\chi^2}{M^4 c_\chi} (m^2 - \mu_2^2)$	$-s_\chi^2 + \xi \frac{2s_\chi^2}{M^2} (m^2 - \mu_2^2)$ $+\xi^2 \frac{s_\chi^2}{3c_\chi M^4} (m^2 - \mu_2^2) \left[m^2 (13s_\chi^2 \right.$ $\left. - 10) + \mu_2^2 (16 - 19s_\chi^2) \right]$

Table 1: HEFT couplings for the Z2RSE. All the couplings are shown up to $\mathcal{O}(\xi^2)$.

2.2 CSE

The model

We now turn to the CSE [79–81]. We follow ref. [82], and thus include neither a Z_2 , nor a $U(1)$ symmetry. The starting point is again the SM, and we add to it a complex scalar singlet, S_c . We write the potential as:

$$V = -\frac{\mu^2}{2} \phi^\dagger \phi + \frac{\lambda}{4} (\phi^\dagger \phi)^2 + \frac{1}{2} b_2 |S_c|^2 + \frac{\delta_2}{2} \phi^\dagger \phi |S_c|^2 + \frac{1}{4} d_2 (|S_c|^2)^2 + \left[a_1 S_c + \frac{1}{4} b_1 S_c^2 + \frac{1}{6} e_1 S_c^3 \right.$$

$$\left. + \frac{1}{6} e_2 S_c |S_c|^2 + \frac{1}{8} d_1 S_c^4 + \frac{1}{8} d_3 S_c^2 |S_c|^2 + \frac{1}{4} \delta_1 \phi^\dagger \phi S_c + \frac{1}{4} \delta_3 \phi^\dagger \phi S_c^2 + \text{h.c.} \right], \quad (18)$$

where μ^2 , λ , d_2 , δ_2 and b_2 are real, while the other parameters are complex. The fields are written as:³

$$\phi = \begin{pmatrix} G^+ \\ \frac{1}{\sqrt{2}} (v + h + iG_0) \end{pmatrix}, \quad S_c = \frac{S + iA}{\sqrt{2}}, \quad (19)$$

³ S_c could have a (complex) vev, but this can be set to zero without loss of generality [82].

where v , G_0 and G^+ have the same meaning as for the Z2RSC, and h , S and A are real neutral fields, not yet mass states. Requiring them to be free from tadpoles leads to the minimization equations:

$$\mu^2 = \frac{\lambda}{2}v^2, \quad a_1 = -\frac{\delta_1}{8}v^2. \quad (20)$$

Then, h , S and A can be diagonalized introducing the mixing angles θ_1 and θ_2 , obeying:⁴

$$\begin{pmatrix} h_1 \\ h_2 \\ h_3 \end{pmatrix} = \begin{pmatrix} c_{\theta_1} & -s_{\theta_1} & 0 \\ s_{\theta_1}c_{\theta_2} & c_{\theta_1}c_{\theta_2} & s_{\theta_2} \\ s_{\theta_1}s_{\theta_2} & c_{\theta_1}s_{\theta_2} & -c_{\theta_2} \end{pmatrix} \begin{pmatrix} h \\ S \\ A \end{pmatrix}, \quad (21)$$

where the fields h_i ($i = 1, 2, 3$) are mass states with mass m_i , such that $m_1 \equiv m = 125$ GeV. The model thus contains, besides the SM particles, two heavy real scalars h_2 and h_3 . Taking λ, δ_1, b_1 and b_2 as dependent parameters, their expressions in terms of the independent parameters read:

$$\lambda = \frac{2}{v^2} \left[m_1^2 c_1^2 + s_1^2 (m_2^2 c_2^2 + m_3^2 s_2^2) \right], \quad (22a)$$

$$\delta_{1R} = \frac{\sqrt{2} s_1 c_1}{v} \left[m_2^2 + m_3^2 - 2m_1^2 + (m_2^2 - m_3^2)(c_2^2 - s_2^2) \right], \quad (22b)$$

$$\delta_{1I} = \frac{2\sqrt{2} s_1 s_2 c_2}{v} (m_3^2 - m_2^2), \quad (22c)$$

$$b_{1R} = -\frac{\delta_{3R} v^2}{2} + m_1^2 s_1^2 + c_2^2 (m_2^2 c_1^2 - m_3^2) + s_2^2 (m_3^2 c_1^2 - m_2^2), \quad (22d)$$

$$b_{1I} = 2 c_1 s_2 c_2 (m_3^2 - m_2^2) - \frac{\delta_{3I} v^2}{2}, \quad (22e)$$

$$b_2 = m_1^2 s_1^2 + c_2^2 (m_2^2 c_1^2 + m_3^2) + s_2^2 (m_3^2 c_1^2 + m_2^2) - \frac{\delta_2 v^2}{2}, \quad (22f)$$

where we used the notation $x_R = \text{Re}(x)$ and $x_I = \text{Im}(x)$, for any x . In the following, we take h_2 and h_3 to be degenerate, and define $M = m_2 = m_3$. The set of independent parameters of the scalar sector then is:

$$v, m, M, \theta_1, \theta_2, \delta_2, \delta_3, d_1, d_2, d_3, e_1, e_2. \quad (23)$$

Restrictions

Similarly to the Z2RSE, we restrict the parameter space of the CSE by taking into account electroweak precision measurements, perturbative unitarity, the perturbativity of the quartic couplings, boundedness of the potential from below, Higgs coupling measurements, and searches for heavy scalars [83]. We follow ref. [84] in using the constraint $|s_1| \lesssim 0.2$ and consider $M \sim 800$ GeV. The parameter points chosen for our numerical results satisfy all of these constraints. We do not make the assumption that one of the scalars is a dark matter candidate as is frequently done [85].

Power countings

All the PCs that we consider for the CSE take eq. (23) as the set of independent parameters, such that:

- PC_1^C imposes the decoupling scaling:

$$M^2 \sim \mathcal{O}(\xi^{-1}), \quad s_1 \sim \mathcal{O}(\xi). \quad (24)$$

⁴The diagonalization matrix could have a third mixing angle, which can be removed without loss of generality [82].

- PC_2^{C} imposes:

$$M^2 \sim \mathcal{O}(\xi^{-1}), \quad s_1^2 \sim \mathcal{O}(\xi), \quad e_1^2 \sim \mathcal{O}(\xi^{-1}), \quad e_2^2 \sim \mathcal{O}(\xi^{-1}). \quad (25)$$

- PC_3^{C} imposes:

$$M^2 \sim \mathcal{O}(\xi^{-1}). \quad (26)$$

As before, all these PCs represent consistent approaches to an EFT. The cubic terms, e_1, e_2 and δ_1 , all have the dimensions of mass in this case. As a consequence, they can potentially scale in different ways in the limit of large M . This ambiguity is intrinsically present in the matching of the model to the HEFT. Concerning the three PCs chosen in eqs. (24) to (26), PC_1^{C} is the decoupling PC. From eq. (22a), indeed, the scaling (24) implies that λ does not scale with negative powers of ξ . This does not happen in PC_2^{C} or PC_3^{C} . The latter performs an expansion only in inverse powers of M . The former not only imposes a stronger scaling for s_1 than PC_1^{C} , but also exploits the fact that e_1 and e_2 are dimensionful parameters to scale them as heavy. We checked that, in the processes discussed here, the trivial order (ξ^0) of PC_2^{C} corresponds to the SM, and the existence of odd powers of s_χ, e_1 and e_2 does not introduce non-integers powers of ξ in the expansion (as odd powers of e_i always multiply odd powers of s_1).

The matching results for the different PCs are shown in table 2, where we define $\bar{\delta}_{23} \equiv \delta_2 + \delta_{3\text{R}}$ and $e_{12\text{R}} \equiv e_{1\text{R}} + e_{2\text{R}}$. As before, we present the results up to $\mathcal{O}(\xi^2)$ (writing explicitly the powers of ξ), except in the cases for which the expressions are too lengthy. In those cases, we indicate the order of the terms not included. The complete matching results up to $\mathcal{O}(\xi^2)$ can be found in the auxiliary file accompanying this manuscript. As in the Z2RSE, all Δx vanish in the alignment limit, $s_1 = 0$.

PC	Δa	Δb	$\Delta \kappa_3$	$\Delta \kappa_4$
PC_1^{C}	$-\xi^2 \frac{s_1^2}{2}$	$-\xi^2 2s_1^2$	$\xi^2 \frac{s_1^2}{2m_1^2} (v^2 \bar{\delta}_{23} - 3m_1^2)$	$\xi^2 \frac{s_1^2}{3m_1^2} (9v^2 \bar{\delta}_{23} - 25m_1^2)$
PC_2^{C}	$-\xi \frac{s_1^2}{2}$ $-\xi^2 \frac{s_1^4}{8}$	$-\xi 2s_1^2$ $+\mathcal{O}(\xi^2)$	$-\xi \frac{s_1^2}{6m_1^2} (9m_1^2 - 3v^2 \bar{\delta}_{23} + \sqrt{2}s_1 v e_{12\text{R}})$ $+\xi^2 \frac{s_1^4}{8m_1^2} (3m_1^2 - 2v^2 \bar{\delta}_{23})$	$\xi \frac{s_1^2}{3m_1^2} (9v^2 \bar{\delta}_{23} - 3\sqrt{2}s_1 v e_{12\text{R}} - 25m_1^2) + \mathcal{O}(\xi^2)$
PC_3^{C}	$c_1 - 1$	$c_1^4 - 1$ $+\mathcal{O}(\xi)$	$-\frac{v}{24m_1^2} [3c_1 v (c_1^2 - 3s_1^2 - 1) \bar{\delta}_{23} + \sqrt{2}s_1 (-3c_1^2 + s_1^2 + 3)e_{12\text{R}}]$ $+\frac{c_1}{4} (c_1^2 - 3s_1^2 + 3) - 1$	$\frac{s_1^2 v}{2m_1^2} [s_1^2 v (-6(c_1^2 + 1) \bar{\delta}_{23} + d_{13\text{R}} + d_2) + 6v \bar{\delta}_{23} - 2\sqrt{2}c_1^3 s_1 e_{12\text{R}}]$ $+c_1^4 \left(1 - \frac{19s_1^2}{3}\right) - 1 + \mathcal{O}(\xi)$

Table 2: HEFT couplings for the CSE. All the couplings are shown up to $\mathcal{O}(\xi^2)$, except the ones that are too lengthy. The full expressions can be found in the auxiliary file.

2.3 2HDM

The model

As a final example, we consider the 2HDM [86] (for reviews, see e.g. refs. [87, 88]); we follow ref. [89] closely. The 2HDM is built starting again with the SM (whose Higgs doublet we now identify as Φ_1) and adding a second Higgs doublet, Φ_2 . We take their vevs to be $v_1/\sqrt{2}$ and $v_2/\sqrt{2}$, respectively, both of which are assumed to be real. A Z_2 symmetry is imposed, according to which $\Phi_1 \rightarrow \Phi_1, \Phi_2 \rightarrow -\Phi_2$. If the Z_2 symmetry is exact, the model does not have a decoupling limit. The symmetry is assumed to be softly broken, which means that bilinear terms that violate the symmetry are allowed. The potential of the theory thus reads:

$$V_{\text{2HDM}} = m_{11}^2 \Phi_1^\dagger \Phi_1 + m_{22}^2 \Phi_2^\dagger \Phi_2 - m_{12}^2 [\Phi_1^\dagger \Phi_2 + \Phi_2^\dagger \Phi_1] + \frac{\lambda_1}{2} (\Phi_1^\dagger \Phi_1)^2 + \frac{\lambda_2}{2} (\Phi_2^\dagger \Phi_2)^2 + \lambda_3 (\Phi_1^\dagger \Phi_1) (\Phi_2^\dagger \Phi_2) + \lambda_4 (\Phi_1^\dagger \Phi_2) (\Phi_2^\dagger \Phi_1) + \frac{\lambda_5}{2} [(\Phi_1^\dagger \Phi_2)^2 + (\Phi_2^\dagger \Phi_1)^2], \quad (27)$$

with all parameters real.⁵ It is convenient to consider a different basis — the Higgs basis [91–94] — with doublets H_1 and H_2 defined by:

$$\begin{pmatrix} H_1 \\ H_2 \end{pmatrix} = \begin{pmatrix} c_\beta & s_\beta \\ -s_\beta & c_\beta \end{pmatrix} \begin{pmatrix} \Phi_1 \\ \Phi_2 \end{pmatrix}, \quad (28)$$

with β defined such that $t_\beta = v_2/v_1$. In the Higgs basis, the potential reads:

$$V_{\text{2HDM}} = Y_1 H_1^\dagger H_1 + Y_2 H_2^\dagger H_2 + Y_3 (H_1^\dagger H_2 + \text{h.c.}) + \frac{Z_1}{2} (H_1^\dagger H_1)^2 + \frac{Z_2}{2} (H_2^\dagger H_2)^2 + Z_3 (H_1^\dagger H_1) (H_2^\dagger H_2) + Z_4 (H_1^\dagger H_2) (H_2^\dagger H_1) + \left\{ \frac{Z_5}{2} (H_1^\dagger H_2)^2 + Z_6 (H_1^\dagger H_1) (H_1^\dagger H_2) + Z_7 (H_2^\dagger H_2) (H_1^\dagger H_2) + \text{h.c.} \right\}, \quad (29)$$

where all parameters are again real. The Higgs doublets are parametrized as:

$$H_1 = \begin{pmatrix} G^+ \\ \frac{1}{\sqrt{2}} (v + h_1^H + iG_0) \end{pmatrix}, \quad H_2 = \begin{pmatrix} H^+ \\ \frac{1}{\sqrt{2}} (h_2^H + iA) \end{pmatrix}, \quad (30)$$

where $v \equiv \sqrt{v_1^2 + v_2^2} = 246 \text{ GeV}$, H^+ and A are respectively the charged and CP-odd neutral scalars with masses m_{H^\pm} and m_A , respectively. h_1^H and h_2^H do not have well-defined masses; the physical states h and H — with masses $m = 125 \text{ GeV}$ and m_H , respectively — can be obtained from those two states via the introduction of a new mixing angle, α , so that:

$$\begin{pmatrix} h \\ H \end{pmatrix} = \begin{pmatrix} s_{\beta-\alpha} & c_{\beta-\alpha} \\ c_{\beta-\alpha} & -s_{\beta-\alpha} \end{pmatrix} \begin{pmatrix} h_1^H \\ h_2^H \end{pmatrix}. \quad (31)$$

We assume $0 \leq \beta - \alpha \leq \pi$, so that $s_{\beta-\alpha} = \sqrt{1 - c_{\beta-\alpha}^2} > 0$. In the following, we take all heavy masses to be degenerate and define $M \equiv m_H = m_A = m_{H^\pm}$.⁶ One possible choice of independent parameters of the scalar sector is the following:

$$c_{\beta-\alpha}, \beta, v, m, Y_2, M. \quad (32)$$

⁵ m_{12}^2 and λ_5 can in general be complex. Taking them to be real implies that CP is conserved in the scalar sector of the theory at tree-level. It should be clear, however, that this is but a particular solution of the model with CP violation in the scalar sector, and not a model in itself [90].

⁶For details on the general case of non-degenerate heavy masses, see ref. [38].

Another choice is the set which replaces Y_2 by m_{12}^2 as an independent parameter:

$$c_{\beta-\alpha}, \beta, v, m, m_{12}^2, M. \quad (33)$$

The Z_2 symmetry is extended to the fermionic sector to avoid flavor-changing neutral currents at tree-level. This extension can be applied in four different ways, each one leading to a different type of 2HDM (for details, see e.g. ref. [89]). In this paper, we consider only the Type-I, as it is the most interesting type from an EFT perspective [89]. Two Feynman rules that are relevant in the discussion of section 3.3 are:

$$\begin{aligned}
& \text{Left diagram: } h \text{ (dashed) } \rightarrow b \text{ (solid) } + b \text{ (solid)} \quad -i \frac{m_b}{v} \frac{1}{\tan \beta} (c_{\beta-\alpha} + s_{\beta-\alpha} \tan \beta), \\
& \text{Right diagram: } h \text{ (dashed) } \rightarrow W_\rho^- \text{ (wavy) } + W_\nu^+ \text{ (wavy)} \quad i \frac{2m_W^2}{v} s_{\beta-\alpha} g_{\rho\nu}.
\end{aligned} \quad (34)$$

Finally, the expressions for $h \rightarrow \gamma\gamma$ and $h \rightarrow \gamma Z$ can be found e.g. in refs. [95] and [87].

Restrictions

The 2HDM is experimentally constrained by many results, including LHC data for the 125 GeV scalar, searches for heavy scalars, Higgs coupling measurements and B meson decays [96]. Constraints resulting from the contribution of H^+ to $b \rightarrow s\gamma$ force $\tan \beta \geq 1.2$ [97]. On the theoretical side, we restrict ourselves to regions of the parameter space complying with boundedness of the potential from below, perturbative unitarity [98–100] and precision electroweak measurements. We use the analysis of ref. [38] to determine the maximum value of $|c_{\beta-\alpha}|$ allowed for the different values of $\tan \beta$, Y_2 and M .

Power countings

We consider the following possible PCs for an EFT matched to the 2HDM:

- PC_1^T takes eq. (32) as the set of independent parameters, and imposes the decoupling scaling:

$$Y_2 \sim \mathcal{O}(\xi^{-1}), \quad M^2 = Y_2 + \mathcal{O}(\xi^0) \sim \mathcal{O}(\xi^{-1}), \quad c_{\beta-\alpha} \sim \mathcal{O}(\xi). \quad (35)$$

- PC_2^T takes eq. (32) as the set of independent parameters, and imposes:

$$Y_2 \sim \mathcal{O}(\xi^{-2}), \quad M^2 \sim \mathcal{O}(\xi^{-2}), \quad c_{\beta-\alpha} \sim \mathcal{O}(\xi). \quad (36)$$

- PC_3^T takes eq. (33) as the set of independent parameters, and imposes:

$$M^2 \sim \mathcal{O}(\xi^{-1}). \quad (37)$$

As before, all PCs are theoretically consistent, as they do not induce negative powers of ξ in the effective Lagrangian. PC_1^T is the PC used in ref. [38] and is the decoupling PC [101, 102]; for details, see ref. [38]. Given that Y_2 is the parameter that ensures decoupling when taken to be very large, its choice as an

independent parameter is reasonable in the decoupling scenario. This choice requires $c_{\beta-\alpha}$ to be small, or else the h^3 coupling would scale with negative powers of ξ [38]. This means, in particular, that the choice of eq. (32) as the set of independent parameters does not allow a consistent expansion solely in terms of M [38]. PC_2^{T} is similar to PC_1^{T} , except that Y_2 and the physical heavy masses squared are required to be enhanced by an extra inverse power of the expansion parameter ξ . Finally, PC_3^{T} is the PC put forward in ref. [39]; it takes advantage of the set of independent parameters (33) to avoid scaling $c_{\beta-\alpha}$. With eq. (33), indeed, the h^3 coupling is well-behaved, as it does not depend on positive powers of M . This allows an EFT expansion solely in terms of M . In particular, $c_{\beta-\alpha}$ does not scale with ξ in PC_3^{T} . Note also that, in the HEFT Lagrangian with PC_3^{T} , the $h\bar{b}b$ coupling is identical to that of the full 2HDM model (as a consequence not only of the Feynman rule for that interaction in eq. (34), but also of the fact that PC_3^{T} does not scale $c_{\beta-\alpha}$).

The matching of the 2HDM to HEFT for the PCs of eqs. (35), (36) and (37) is given in tables 3 and 4, where we define $\bar{m}_{12}^2 \equiv m_{12}^2/(m_h^2 s_\beta c_\beta)$ and $t_\beta \equiv \tan\beta$. In PC_1^{T} , we write the expressions in the general case where the heavy masses are not necessarily degenerate. More specifically, we follow ref. [38] and introduce the real quantities Δm_H^2 , Δm_A^2 and Δm_{H+} , such that $m_H^2 = Y_2 + \Delta m_H^2$, $m_A^2 = Y_2 + \Delta m_A^2$, $m_{H+}^2 = Y_2 + \Delta m_{H+}^2$. The results for PC_3^{T} agree with those of ref. [39].

PC	Δb	$\Delta \kappa_3$	$\Delta \kappa_4$
PC_1^T	$-\xi^2 3c_{\beta-\alpha}^2$	$-\xi 2c_{\beta-\alpha}^2 \frac{Y_2}{m_h^2} + \xi^2 \frac{1}{2} c_{\beta-\alpha}^2$	$-\xi 12c_{\beta-\alpha}^2 \frac{Y_2}{m_h^2} + \xi^2 c_{\beta-\alpha}^2 \left(\frac{16\Delta m_H^2}{m_h^2} - 11 \right)$
PC_2^T	$-\xi^2 3c_{\beta-\alpha}^2$	$-\frac{2Y_2 c_{\beta-\alpha}^2}{m_h^2} + \xi \frac{c_{\beta-\alpha}^3}{m_h^2 t_\beta} (t_\beta^2 - 1)(Y_2 - M^2)$ $+ \xi^2 \frac{c_{\beta-\alpha}^2}{2m_h^2 t_\beta^2} \left(c_{\beta-\alpha}^2 \left[M^2(t_\beta^4 - 4t_\beta^2 + 1) + 2Y_2 t_\beta^2 \right] \right.$ $\left. + m_h^2 t_\beta^2 \right)$	$\frac{4Y_2 c_{\beta-\alpha}^2}{m_h^2 M^2} (M^2 - 4Y_2)$ $+ \xi \frac{2c_{\beta-\alpha}^3}{m_h^2 M^2 t_\beta} (t_\beta^2 - 1) (M^2 - 12Y_2) (M^2 - Y_2)$ $+ \mathcal{O}(\xi^2)$
PC_3^T	$c_{\beta-\alpha}^2 \left(1 - 2c_{\beta-\alpha}^2 \right.$ $\left. + 2c_{\beta-\alpha} s_{\beta-\alpha} \cot 2\beta \right)$ $+ \mathcal{O}(\xi)$	$-1 + s_{\beta-\alpha} (1 + 2c_{\beta-\alpha}^2) + c_{\beta-\alpha}^2 \left[-2s_{\beta-\alpha} m_{12}^2 \right.$ $\left. + 2c_{\beta-\alpha} \cot 2\beta (1 - m_{12}^2) \right]$	$\frac{c_{\beta-\alpha}^2}{3} \left(-7 + 64c_{\beta-\alpha}^2 - 76c_{\beta-\alpha}^4 + 12(1 - 6c_{\beta-\alpha}^2 + 6c_{\beta-\alpha}^4) \bar{m}_{12}^2 \right.$ $+ 4c_{\beta-\alpha} s_{\beta-\alpha} \cot 2\beta \left[-13 + 38c_{\beta-\alpha}^2 - 3(-5 + 12c_{\beta-\alpha}) \bar{m}_{12}^2 \right]$ $\left. + 4c_{\beta-\alpha}^2 \cot^2 2\beta \left[3c_{\beta-\alpha}^2 - 16s_{\beta-\alpha}^2 + 3(-1 + 6s_{\beta-\alpha}^2) \bar{m}_{12}^2 \right] \right)$ $+ \mathcal{O}(\xi)$

Table 3: b , κ_3 and κ_4 HEFT couplings for the 2HDM. All the couplings are shown up to $\mathcal{O}(\xi^2)$, except the ones that are too lengthy. The full expressions can be found in the auxiliary file.

PC	Δa	Δc_1	$a_{h\gamma\gamma}$	$a_{h\gamma Z}$
PC_1^T	$-\xi^2 \frac{c_{\beta-\alpha}^2}{2}$	$\xi \frac{c_{\beta-\alpha}}{\tan \beta} - \xi^2 \frac{c_{\beta-\alpha}^2}{2}$	$-\xi \frac{\Delta m_H^2}{48\pi^2 Y_2} + \mathcal{O}(\xi^2)$	$\xi \frac{\Delta m_{H+}^2 (m_Z^2 - 2m_W^2)}{96\pi^2 m_W^2 Y_2} + \mathcal{O}(\xi^2)$
PC_2^T	$-\xi^2 \frac{c_{\beta-\alpha}^2}{2}$	$\xi \frac{c_{\beta-\alpha}}{\tan \beta} - \xi^2 \frac{c_{\beta-\alpha}^2}{2}$	$\frac{1}{48\pi^2 Y_2} (Y_2 - M^2) + \xi \frac{c_{\beta-\alpha} \cot 2\beta}{48\pi^2 M^2} (Y_2 - M^2) + \mathcal{O}(\xi^2)$	$-\frac{(M^2 - Y_2) (2m_W^2 - m_Z^2)}{96\pi^2 M^2 m_W^2} - \xi \frac{\cot(2\beta) (M^2 - Y_2) c_{\beta-\alpha} (2m_W^2 - m_Z^2)}{96\pi^2 M^2 m_W^2} + \mathcal{O}(\xi^2)$
PC_3^T	$s_{\beta-\alpha} - 1$	$\frac{1}{\tan \beta} \left(\frac{c_{\beta-\alpha}}{\tan \beta s_{\beta-\alpha}} \right) - 1$	$-\frac{s_{\beta-\alpha}}{48\pi^2} + \xi \frac{m_{12}^2}{48\pi^2 M^2} \csc(\beta) \sec(\beta) \left(\cot(2\beta) c_{\beta-\alpha} + \frac{s_{\beta-\alpha}}{s_{\beta-\alpha}} \right) - \xi \frac{m_h^2}{1440\pi^2 M^2} \left(30 \cot(2\beta) c_{\beta-\alpha} + 19 s_{\beta-\alpha} \right) + \mathcal{O}(\xi^2)$	$\frac{s_{\beta-\alpha}}{96m_W^2 \pi^2} (m_Z^2 - 2m_W^2) - \xi \frac{(2m_W^2 - m_Z^2)}{2880\pi^2 M^2 m_W^2} \left[30 \cot(2\beta) c_{\beta-\alpha} (m_h^2 - m_{12}^2 \csc(\beta) \sec(\beta)) + s_{\beta-\alpha} (19m_h^2 - 30m_{12}^2 \csc(\beta) \sec(\beta) + 2m_Z^2) \right] + \mathcal{O}(\xi^2)$

Table 4: a , $a_{h\gamma\gamma}$ and $a_{h\gamma Z}$ HEFT couplings for the 2HDM. All the couplings are shown up to $\mathcal{O}(\xi^2)$, except the ones that are too lengthy. The full expressions can be found in the auxiliary file.

3 Numerical results

The results that follow were obtained via FEYNMASTER [103,104] (and its accompanying software [105–110]), as well as FEYNARTS [111] and FORMCALC [112]. The results will be shown in the range allowed by the theoretical constraints of the model being considered. For each model, we compare the results of the full UV model with those of the PCs introduced in the previous section. Unless mentioned otherwise, all results coincide in the alignment limit ($s_\chi = 0$ in the Z2RSE, $s_1 = 0$ in the CSE and $c_{\beta-\alpha} = 0$ in the 2HDM), which is also the SM result.⁷

3.1 Z2RSE

In fig. 1, we present the differential cross section $hh \rightarrow hh$, for two different values of the center of mass energy: $\sqrt{s} = 300$ GeV (left panel) and $\sqrt{s} = 600$ GeV (right panel). Let us start by discussing the

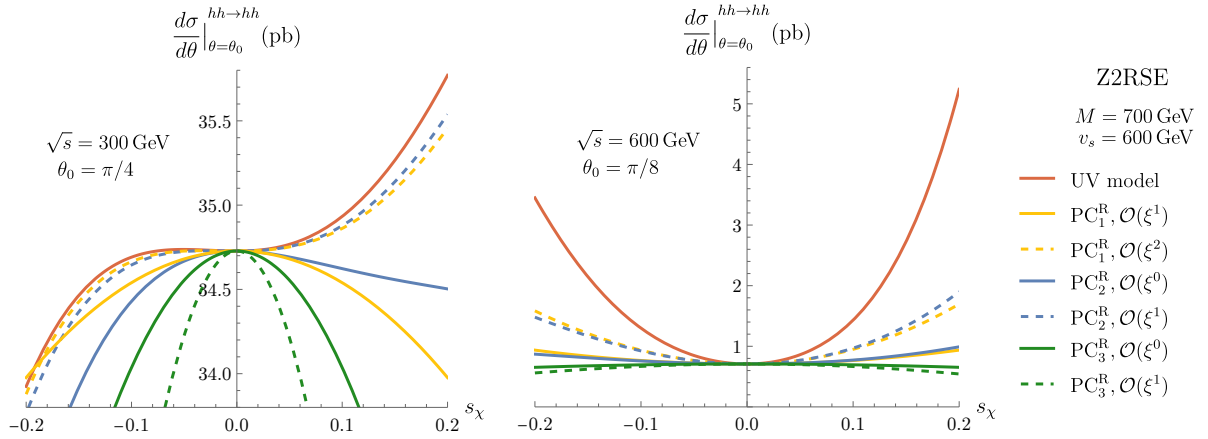


Figure 1: Comparison between the complete Z2RSE and the HEFT approaches to it in the differential cross-section of $hh \rightarrow hh$, for a center-of-mass energy \sqrt{s} and a scattering angle θ_0 .

left panel. We find two very relevant features. The first one concerns the difference between PC_2^{R} and PC_3^{R} . Recall that these PCs both perform an expansion simply in terms of the heavy mass M , and differ only in the choice of independent parameters. Still, the left panel of fig. 1 shows that they lead to radically different results. Indeed, whereas PC_2^{R} clearly converges to the UV model result as higher orders in ξ are considered (such that the $\mathcal{O}(\xi^1)$ result is a very good replication), PC_3^{R} is utterly unable to properly describe the full model away from the alignment limit, $s_\chi = 0$, for the both orders shown.⁸ This demonstrates not only that the HEFT matching is not unique, but also that making different choices of independent parameters may be crucially important.

Also very interesting on the left panel of fig. 1 is the comparison between PC_1^{R} and PC_2^{R} . As discussed above, the latter is the PC introduced in ref. [60] to describe the HEFT approach to the Z2RSE, whereas the former is the decoupling PC (to recap, $\mathcal{O}(\xi^1)$ and $\mathcal{O}(\xi^2)$ of PC_1^{R} correspond to SMEFT dimension-6 and dimension-8, respectively). The panel shows that, in the region of $s_\chi < 0$, PC_1^{R} outperforms PC_2^{R} . This holds for both orders shown: the SMEFT dimension-6 (8) result is closer to the Z2RSE one than

⁷The only exceptions will be the loop processes $h \rightarrow \gamma\gamma$ and $h \rightarrow \gamma Z$ in the 2HDM.

⁸We checked that the results eventually improve when PC_3^{R} $\mathcal{O}(\xi^2)$ is considered.

the $\mathcal{O}(\xi^0)$ ($\mathcal{O}(\xi^1)$) result of PC_2^{R} . One should keep in mind, however, that in terms of the ξ expansion, the first non-trivial order in the PC_1^{R} expansion is one order higher than the first non-trivial order in the PC_2^{R} expansion (since $\mathcal{O}(\xi^0)$ in PC_1^{R} corresponds to the SM case). Nevertheless, this plot provides an example where a SMEFT approach might be more convenient to reproduce the full model than a (HEFT) approach which only scales the physical heavy masses.

The right panel of fig. 1 illustrates a scenario where the EFT expansion starts to break down, as the energies of the problem are very close to those of the UV theory.⁹ Accordingly, whereas the differences between PC_2^{R} at $\mathcal{O}(\xi^1)$ and the Z2RSE were around 1% on the left plot, the differences are larger than 50% on the right plot. It is also clear that, for $s_\chi < 0$, PC_1^{R} still constitutes a more rapid approach to the full model than PC_2^{R} , which also shows that such a conclusion does not depend on the energy of the problem. Finally, the results for PC_3^{R} are closer to those of the other PCs than on the left panel.

In fig. 2, we present similar plots, but now for the scattering $WW \rightarrow hh$. Both panels show essentially the same features as those of the corresponding plot of fig. 1 (except that, on the left plot of fig. 2, PC_3^{R} at $\mathcal{O}(\xi^1)$ now provides a much more faithful description of the full model). This illustrates that the conclusions derived above are not restricted to the process $hh \rightarrow hh$. Note also that we investigated different regions of the allowed parameter space, and did not find substantially different conclusions.

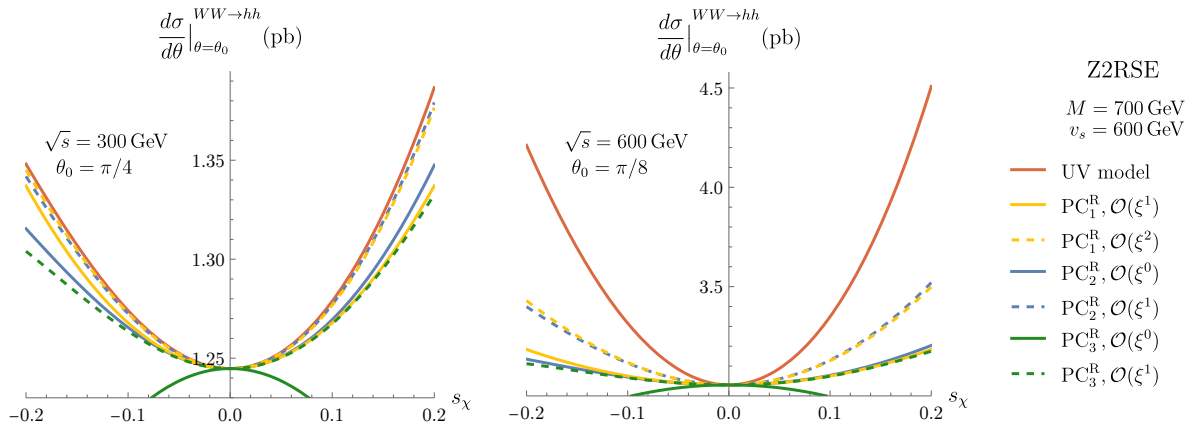


Figure 2: Comparison between the Z2RSE and HEFT approaches to it in the differential cross-section of $WW \rightarrow hh$, for a center-of-mass energy \sqrt{s} and a scattering angle θ_0 .

3.2 CSE

We now discuss the same two scattering processes, but in the context of the CSE. In fig. 3, we show $hh \rightarrow hh$; the two panels consider different points of the parameter space and different scattering conditions. Both plots show the same general features. In particular, the results of the full model are essentially constant in a broad region around the alignment limit, $-0.1 < s_1 < 0.1$. All the three PCs thus easily replicate those results. Away from that region, however, PC_1^{C} (the decoupling PC) displays a very slow convergence to the full model, with both the $\mathcal{O}(\xi^2)$ and $\mathcal{O}(\xi^3)$ yielding a very poor replication of the full model. PC_2^{C} shows a faster convergence, although still with large deviations from the results in shown in

⁹The scattering angle also changes, for illustrative purposes. The conclusions do not change if $\theta_0 = \pi/4$ is used on the right panel.

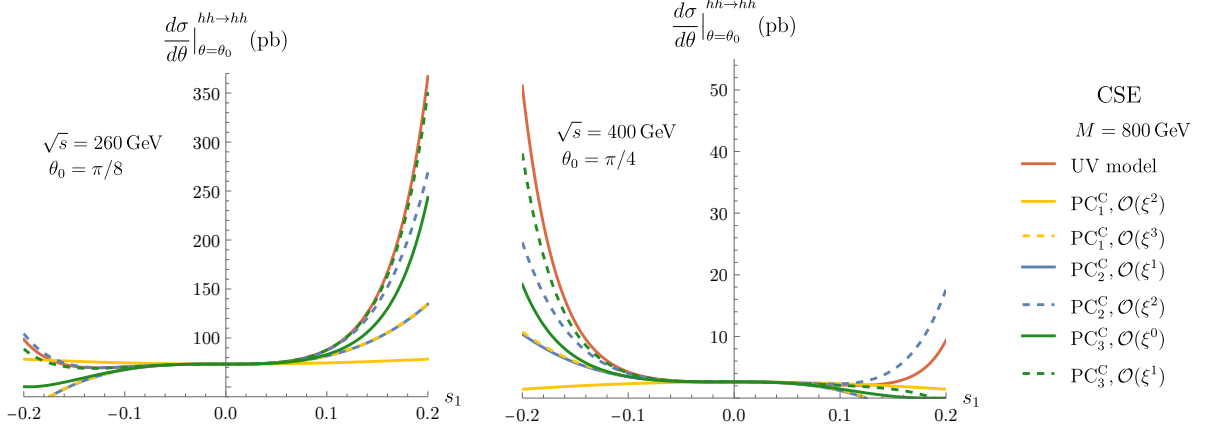


Figure 3: Comparison between the CSE and HEFT approaches to it in the differential cross-section of $hh \rightarrow hh$, for a center-of-mass energy \sqrt{s} and a scattering angle θ_0 . On both panels, we use $\alpha_2 = 0, \delta_2 = 0.765, \delta_3 = 0.695 + i 0.145, d_1 = 0.695 - i 7.63, d_2 = 10.6, d_3 = 1.74 - i 4.77, e_1 = -(28.3 + i 20.4)v, e_2 = -(36.7 - i 68.7)v$. This point is derived from a benchmark point provided in ref. [84].

red. It is only PC_3^{C} that is able to provide satisfactory results away from the alignment limit, immediately at $\mathcal{O}(\xi^1)$.

Similar conclusions hold also for $WW \rightarrow hh$ scattering, which we illustrate in fig. 4 for two different points of the parameter space. Indeed, PC_1^{C} shows again a very slow convergence away from the align-

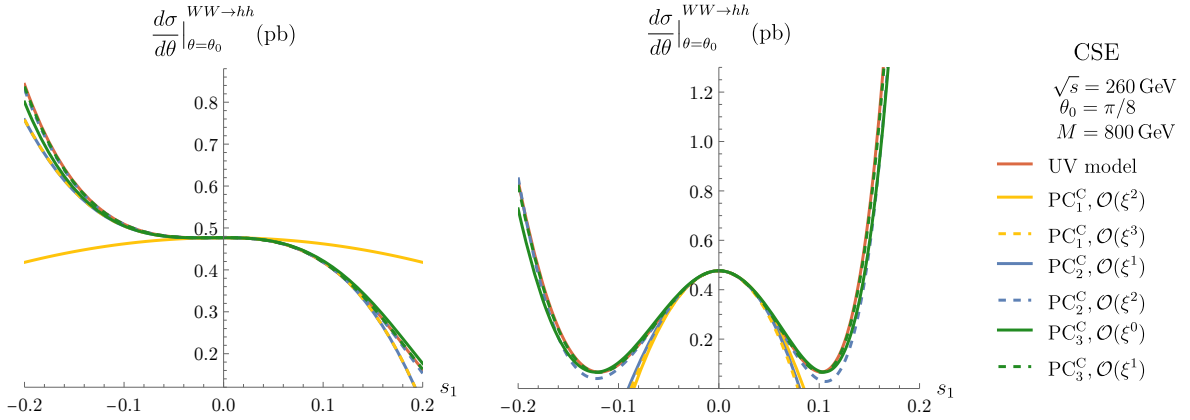


Figure 4: Comparison between the CSE and HEFT approaches to it in the differential cross-section of $WW \rightarrow hh$, for a center-of-mass energy \sqrt{s} and a scattering angle θ_0 . The left panel assumes the point of parameter space of fig. 3, whereas the right plot uses $\alpha_2 = 0, d_2 = 0.611, \delta_2 = 24.6, \delta_3 = 23.5 + i 0.00901, d_1 = -0.0806 + i 0.368, d_3 = -0.128 - i 0.0143, e_1 = -(33 - i 28.5)v, e_2 = -(99.4 + i 91.9)v$. As before, this point is derived from a benchmark point provided in ref. [84].

ment limit. For both $hh \rightarrow hh$ and $WW \rightarrow hh$ scattering, therefore, the SMEFT dimension-8 results (corresponding to PC_1^{C} at $\mathcal{O}(\xi^2)$) are unable to present an accurate description of the full model. Fig. 4 demonstrates that PC_2^{C} has the same pattern in $WW \rightarrow hh$ as in $hh \rightarrow hh$ scattering, with the $\mathcal{O}(\xi^2)$ results having small deviations from the full UV results. Finally, PC_3^{C} is again undisputedly the most adequate PC in both panels of fig. 4, with $\mathcal{O}(\xi^0)$ representing already an excellent description of the CSE results.

3.3 2HDM

In fig. 5, we show the decay width of $h \rightarrow b\bar{b}$ (left panel) and the differential cross-section of $hh \rightarrow hh$ (right panel). In both panels, we compare the result in the 2HDM with those of the three PCs introduced in section 2.3. In the case of $h \rightarrow b\bar{b}$, the PC_3^T result is obviously preferred over the remaining ones; in

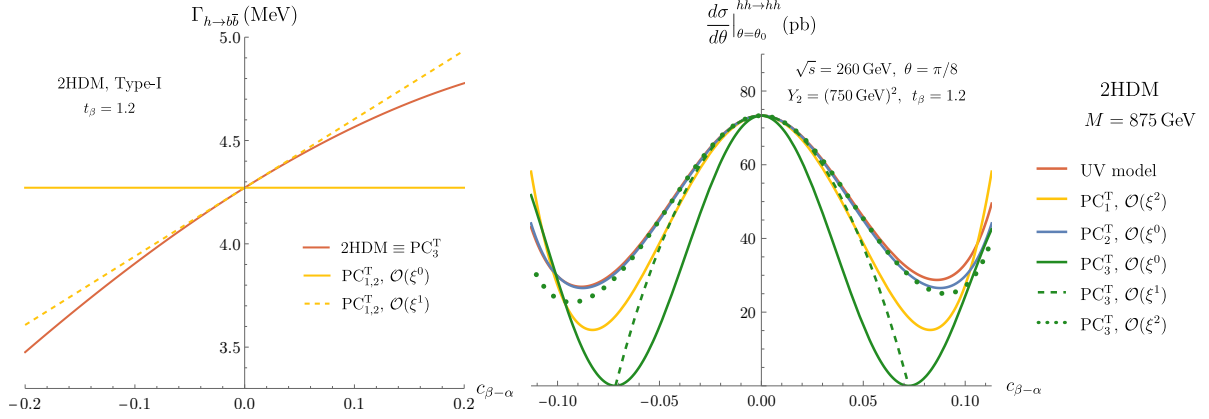


Figure 5: Comparison between the 2HDM and HEFT approaches to it. Left: the decay width of $h \rightarrow b\bar{b}$. Right: differential cross-section of $hh \rightarrow hh$.

fact, as discussed in section 2.3, it exactly replicates the 2HDM result already at $\mathcal{O}(\xi^0)$. PC_1^T and PC_2^T are identical in this process, since only the scaling of $c_{\beta-\alpha}$ determines the result (and that scaling is the same in PC_1^T and PC_2^T). For these two PCs, the $\mathcal{O}(\xi^0)$ result is very poor, as it has no dependence on $c_{\beta-\alpha}$, and is thus a constant equal to the 2HDM result for $c_{\beta-\alpha} = 0$. In other words, the $\mathcal{O}(\xi^0)$ result of PC_1^T and PC_2^T for $h \rightarrow b\bar{b}$ only reproduces the 2HDM in the alignment limit. The $\mathcal{O}(\xi^1)$ result contains a linear dependence on $c_{\beta-\alpha}$, so that it already provides a good reproduction of the 2HDM result within the range of $c_{\beta-\alpha}$ showed.

These results represent a sharp contrast with those of $hh \rightarrow hh$ scattering. In this case, indeed, PC_2^T is by far the most adequate PC. Even though it does not capture the slight asymmetry in $c_{\beta-\alpha}$ of the 2HDM result, it is an excellent approximation to the latter in the entire range of $c_{\beta-\alpha}$ allowed by the theoretical constraints, and immediately at $\mathcal{O}(\xi^0)$. By contrast, PC_3^T represents a poor replication of the 2HDM result away from the alignment limit. This holds not only at $\mathcal{O}(\xi^0)$, but also at $\mathcal{O}(\xi^1)$; the latter improves the quality of the replication of the 2HDM result in the range $-0.05 < c_{\beta-\alpha} < 0.05$, but fails to do so in the remaining range. It is only when the $\mathcal{O}(\xi^2)$ truncation is considered that the PC_3^T result properly approaches the 2HDM result away from the alignment limit — albeit still being worse than PC_2^T at $\mathcal{O}(\xi^0)$. Finally, the yellow curve represents PC_1^T at $\mathcal{O}(\xi^2)$; this result was first shown in ref. [38], and shows a relative difference from the 2HDM larger than 40% for $c_{\beta-\alpha} \simeq 0.08$. The right panel of fig. 5 above thus extends the analysis of that paper, by including two extra PCs.

One might wonder if the results of the right panel of fig. 5 depend significantly on the region of parameter space considered. To address this question, we show in fig. 6 the same observable, but for very different values of Y_2 : $(325 \text{ GeV})^2$ on the left panel, and 0 on right panel. Both scenarios constitute clear deviations from the decoupling limit $Y_2 \gg v^2$. Therefore, the observed failure on both panels of

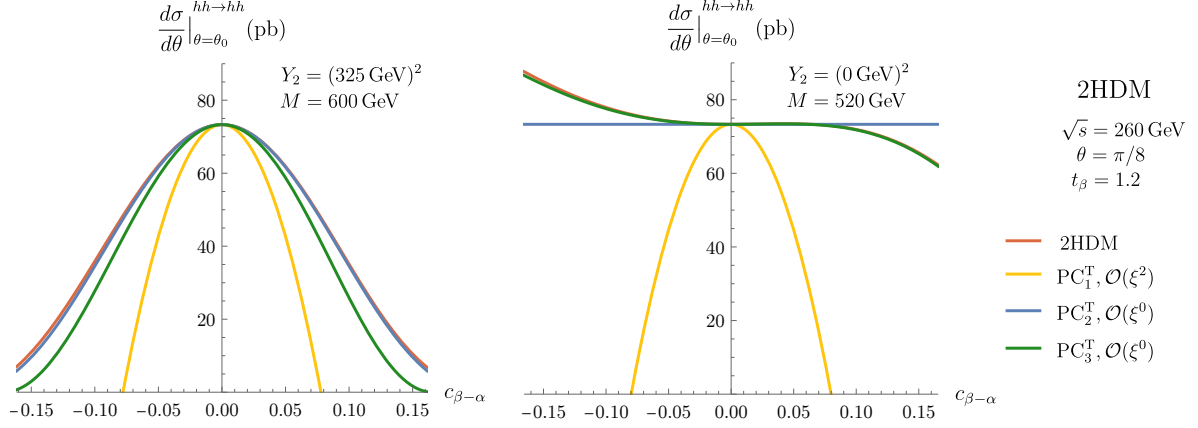


Figure 6: Comparison between the 2HDM and HEFT approaches to it in the differential cross-section of $hh \rightarrow hh$ for non-decoupling scenarios: with $Y_2 = (325 \text{ GeV})^2$ and $M = 600 \text{ GeV}$ (left) and $Y_2 = 0$ and $M = 520 \text{ GeV}$ (right).

PC_1^T (the decoupling PC) to reproduce the 2HDM result away from $c_{\beta-\alpha} = 0$ was expected. As for the other PCs, the figure shows that they are very good replications of the 2HDM. That PC_2^T has such accurate result is surprising, as it imposes the scaling $Y_2 \sim \mathcal{O}(\xi^{-2})$, which thus seems incompatible with very small values of Y_2 . On the other hand, the circumstance that this PC simultaneously imposes the scalings $c_{\beta-\alpha} \sim \mathcal{O}(\xi)$ and $M^2 \sim \mathcal{O}(\xi^{-2})$ compensates for that apparent incompatibility, so that the end result is very accurate. Still, PC_2^T has a less accurate description of the full model than PC_3^T on the right panel of fig. 6. This shows that the conclusions of the right panel of fig. 5 do depend on the region of parameter space considered.

Fig. 7 shows the decay width of $h \rightarrow \gamma\gamma$ (left panel) and $h \rightarrow \gamma Z$ (right panel), again comparing the different possible PCs with the 2HDM result. In both cases, we also show the SM result, which is not obtained by the 2HDM one in the alignment limit $c_{\beta-\alpha} = 0$. This feature is related to the well-known non-

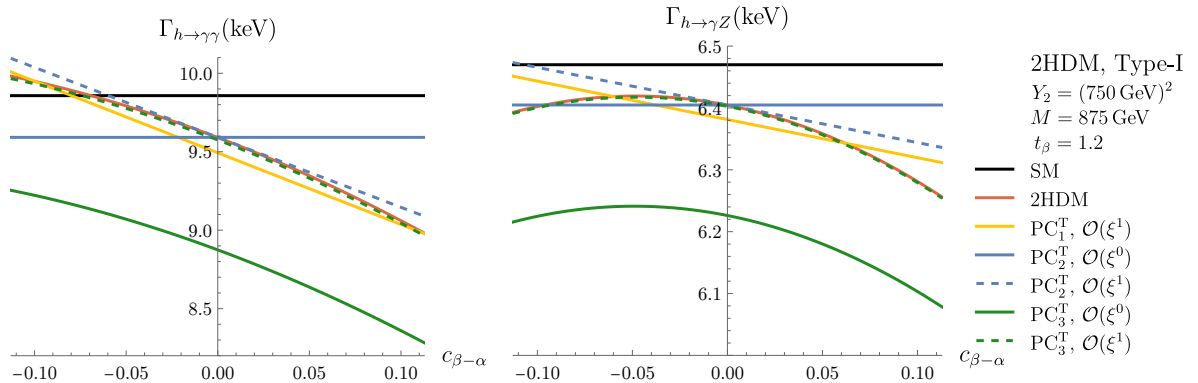


Figure 7: Comparison between the 2HDM and HEFT approaches to it in the decay width of $h \rightarrow \gamma\gamma$ (left) and $h \rightarrow \gamma Z$ (right).

decoupling effects typical of these processes, which are caused by the loop of charged scalars [113–118]. We checked that, in both processes, PC_1^T at $\mathcal{O}(\xi^0)$ generates the SM curve, and not the 2HDM one.

This result is in agreement with the circumstance that PC_1^T is the decoupling PC. The figure shows that PC_1^T presents a reasonable description of the 2HDM already at $\mathcal{O}(\xi^1)$. This means that, even though the loops with charged SM bosons do not contribute at this order (recall eq. 34), the modification of the Yukawa interactions is sufficient to provide a decent replication of the UV model result, albeit with a simple linear dependence on $c_{\beta-\alpha}$. Fig. 7 also shows that PC_3^T at $\mathcal{O}(\xi^0)$ on both panels is quite deviated from the 2HDM result, even in the alignment limit. That curve has an approximately constant relative difference with regards to the 2HDM throughout all the allowed range of $c_{\beta-\alpha}$: around 7% in $h \rightarrow \gamma\gamma$ and around 3% in $h \rightarrow \gamma Z$. On the other hand, PC_3^T at $\mathcal{O}(\xi^1)$ describes an excellent replication of the 2HDM result in both processes. This is not what happens in PC_2^T , which, despite presenting a smaller relative difference to the 2HDM result at $\mathcal{O}(\xi^0)$ (in its constant value), does not provide as adequate an approach to the 2HDM result as PC_3^T at $\mathcal{O}(\xi^1)$.

4 Conclusions

The HEFT can be used at the LHC to parametrize possible deviations from the SM. Eventual non-zero HEFT coefficients should then be converted into coefficients of specific UV models via a matching procedure. In this paper, we noted that such a procedure is not unambiguous. Even if a simple expansion in inverse powers of a heavy mass is used, very different power countings (PCs) are obtained by considering different set of independent parameters. Moreover, different PCs approach the full model differently for different observables. We illustrated these aspects by considering three BSM models with an extended scalar sector: the Z_2 -symmetric real singlet extension (Z2RSE), the complex singlet extension (CSE) and the 2-Higgs Doublet Model (2HDM). For each model, we investigated three PCs, providing the relevant HEFT coefficients. In all the models, one of the PCs chosen is the decoupling PC, in the sense that it leads to the same results as the SMEFT.

In the Z2RSE, we showed that two PCs that perform an expansion just in inverse powers of the heavy physical mass lead to very different results, due to different choices for the independent parameters. We also showed regions where both approach the full theory less rapidly than the SMEFT results. In the CSE, the decoupling PC leads to a very slow convergence, so that even the SMEFT dimension-8 results are inadequate to replicate the full model away from the alignment limit. Finally, in the 2HDM, we illustrated how different PCs are more accurate for different observables. For example, while the PC identified as PC_3^T is most adequate for 2 body decays of the Higgs boson, PC_2^T is clearly more accurate for some regions of processes such as $hh \rightarrow hh$. We also showed that an intuition for the performance of a PC is not always available, as PC_2^T properly replicates the 2HDM for very low values of Y_2 , even though it scales this parameter as a heavy one. As a global conclusion, we note that the existence of multiple theoretically consistent PCs complicates the interpretation of HEFT coefficients in terms of parameters of specific UV models.

This paper is the first exploration of the existence of multiple possible matchings between the HEFT and a UV model. In the future, other models and other processes could be considered, and a systematic comparison between PCs can be put forward. It would be also relevant to investigate the effect of

radiative corrections, and their impact on the consistency of different PCs. An auxiliary file accompanies this manuscript, containing the HEFT couplings for the CSE and the 2HDM.

Acknowledgments

D.F. is grateful to Ilaria Brivio, Supratim Das Bakshi, Howard Haber, Aneesh Manohar and Matthew Sullivan for discussions, as well as to the Mainz Institute for Theoretical Physics (MITP) of the Cluster of Excellence PRISMA+ (Project ID 39083149) for its hospitality and support. C.Q.C and J.J.S.C. are grateful to Gerhard Buchalla for discussions about the singlet extension, and to Francisco Arco, María J. Herrero and Roberto A. Morales for comments on the 2HDM. The authors also thank early conversations with Lucas Barbero. S. D. and D. F. are supported by the U.S. Department of Energy under Grant Contract No. DE-SC0012704. C.Q.C has been funded by the MINECO (Spain) predoctoral grant BES-2017-082408. This work was supported in part by the EU under grant 824093 (STRONG2020), Spanish MICINN under PID2019-108655GB-I00/AEI/10.13039/501100011033, PID2019-106080GB-C21, Universidad Complutense de Madrid under research group 910309 and the IPARCOS institute. This preprint has been issued with number IPARCOS-UCM-23-129.

A HEFT approach to the CSE

In this appendix, we focus on the integration out of the heavy scalars of the CSE, as has already been done for the Z2RSE [60] and the 2HDM [38, 39]. We begin by considering the potential in eq. (18) in terms of the physical states h_1 , h_2 and h_3 . We can split the Lagrangian in the form,

$$\mathcal{L}_{\text{CSE}} = \mathcal{L}_{\text{CSE}}^{\text{light}} + \mathcal{L}_{\text{CSE}}^{\text{heavy}}, \quad (\text{A.1})$$

where $\mathcal{L}_{\text{CSE}}^{\text{light}}$ involves only light (i.e. non-BSM) fields. On the other hand, $\mathcal{L}_{\text{CSE}}^{\text{heavy}}$ involves light and heavy fields, and we can conveniently write it as follows:

$$\mathcal{L}_{\text{CSE}}^{\text{heavy}} = \frac{1}{2}(\partial_\mu H^a)^2 - \frac{1}{2}(M^2)^{ab}H^aH^b + J_1^aH^a + J_2^{ab}H^aH^b + J_3^{abc}H^aH^bH^c + J_4^{abcd}H^aH^bH^cH^d, \quad (\text{A.2})$$

where $(M^2)^{ab}$ is the diagonal squared mass matrix, $H^a = (h_2, h_3)$ are the heavy fields, and the J_k contain only light fields. The heavy scalars H^a are integrated out at tree-level by solving their equations of motion (EoM):

$$J_1^a + (-\partial^2 - M^2 + 2J_2)^{ab}H^b + 3J_3^{abc}H^bH^c + 4J_4^{abcd}H^bH^cH^d = 0. \quad (\text{A.3})$$

As we are only interested in at most $2 \rightarrow 2$ scattering processes at tree level,¹⁰ we neglect terms with more than four fields in $\mathcal{L}_{\text{CSE}}^{\text{light}}$. We also neglect EoM solutions that give rise to terms with more than four light fields in the EFT Lagrangian. Since J_1 and J_2 have at least two and one light fields, respectively, the EoM solutions for $H^a = (h_2, h_3)$ with two fields are fully contained in:

$$\overline{H}^a = \sum_{n=0}^{\infty} (M^{-2-2n})^{ab} \partial^{2n} J_1^b = (M^{-2})^{ab} J_1^b + (M^{-4})^{ab} \partial^2 J_1 + \dots, \quad (\text{A.4})$$

¹⁰Notice that for one-loop amplitudes with three and four external particles, vertices with more than four fields are also in general relevant.

where J_1 has terms with two and three light fields. Note that the full H^a solution for (A.3) has no terms with zero and one fields (it starts with the two-light-field terms in \bar{H}^a). One can thus easily observe that the J_2 and J_3 terms in the Lagrangian (A.2) will give EFT operators with at least five and six fields, as J_2 , and J_3 start with one and zero light fields, respectively. Furthermore, the EFT operators produced by the J_4 term in Lagrangian (A.2) will contain at least eight light fields, where J_4 starts with zero fields. Hence, the resulting EFT operators containing up to four light fields are simply provided by the first line of eq. (A.2):¹¹

$$\mathcal{L}_{\text{CSE}}^{\text{EFT}} \Big|_{\leq 4 \text{ fields}} \subset \mathcal{L}_{\text{CSE}}^{\text{light}} + \frac{1}{2}(\partial_\mu \bar{H}^a)^2 - \frac{1}{2}(M^2)^{ab} \bar{H}^a \bar{H}^b + J_1^a \bar{H}^a. \quad (\text{A.5})$$

Now, it is possible to match this effective Lagrangian with the one given by HEFT in eq. (1). This matching yields the coefficients a , b , κ_3 , and κ_4 of the lowest order HEFT Lagrangian shown in table 2. The expressions for J_1^a up to two light fields are:

$$\begin{aligned} J_1^{h_2} = & \frac{c_2 s_1}{v} (2m_W^2 W_\mu W_\mu^\dagger + m_Z^2 Z_\mu^2) + \frac{h_1^2}{48v} \left(3c_2 s_1^3 (-3v^2 \bar{\delta}_{23} + 4m_h^2 + 2m_2^2) \right. \\ & + 3s_1 v^2 ((9c_1^2 - 1)c_2 \bar{\delta}_{23} - 8c_1 \delta_{31} s_2) + \sqrt{2} s_1^2 v (2s_2 (3e_{1\text{I}} + e_{2\text{I}}) - 9c_1 c_2 e_{12\text{R}}) \\ & \left. + \sqrt{2} (c_1^2 - 1) v (3c_1 c_2 e_{12\text{R}} - 2s_2 (3e_{1\text{I}} + e_{2\text{I}})) - 6(3c_1^2 + 1) c_2 s_1 (2m_h^2 + m_2^2) \right), \end{aligned} \quad (\text{A.6})$$

$$\begin{aligned} J_1^{h_3} = & \frac{s_1 s_2}{v} (2m_W^2 W_\mu W_\mu^\dagger + m_Z^2 Z_\mu^2) + \frac{h_1^2}{48v} \left(-3s_1 v^2 (-9c_1^2 s_2 \bar{\delta}_{23} + (3s_1^2 + 1) s_2 \bar{\delta}_{23} - 8c_2 c_1 \delta_{31}) \right. \\ & + \sqrt{2} v (2c_2 (c_1^2 - s_1^2 - 1) (3e_{1\text{I}} + e_{2\text{I}}) + 3c_1 s_2 (c_1^2 - 3s_1^2 - 1) e_{12\text{r}}) \\ & \left. + 6s_1 s_2 (-3c_1^2 + s_1^2 - 1) (2m_h^2 + m_3^2) \right). \end{aligned} \quad (\text{A.7})$$

¹¹This result is actually general. By construction, indeed, the terms of (A.2) that only contain two heavy fields are included in $(M^2)^{ab}$, while the operators that contain at least one light field in addition to the two heavy ones are given in J_2^{ab} . Moreover, if the H^a particles are mass eigenstates and there are no heavy–light mass mixing terms, J_1^a will always contain at least two light fields. These two are the assumptions that we have employed to extract the 4-field EFT operators in this appendix.

References

- [1] ATLAS Collaboration, G. Aad *et al.*, Phys.Lett. **B716**, 1 (2012), [1207.7214].
- [2] CMS Collaboration, S. Chatrchyan *et al.*, Phys.Lett. **B716**, 30 (2012), [1207.7235].
- [3] S. Weinberg, Phys. Rev. Lett. **43**, 1566 (1979).
- [4] W. Buchmuller and D. Wyler, Nucl. Phys. B **268**, 621 (1986).
- [5] C. N. Leung, S. T. Love and S. Rao, Z. Phys. C **31**, 433 (1986).
- [6] T. Cohen, N. Craig, X. Lu and D. Sutherland, JHEP **03**, 237 (2021), [2008.08597].
- [7] F. Feruglio, Int. J. Mod. Phys. A **8**, 4937 (1993), [hep-ph/9301281].
- [8] J. Bagger *et al.*, Phys. Rev. D **49**, 1246 (1994), [hep-ph/9306256].
- [9] V. Koulovassilopoulos and R. S. Chivukula, Phys. Rev. D **50**, 3218 (1994), [hep-ph/9312317].
- [10] G. Buchalla, O. Catà and C. Krause, Nucl. Phys. B **880**, 552 (2014), [1307.5017], [Erratum: Nucl.Phys.B 913, 475–478 (2016)].
- [11] R. Alonso, M. B. Gavela, L. Merlo, S. Rigolin and J. Yepes, Phys. Lett. B **722**, 330 (2013), [1212.3305], [Erratum: Phys.Lett.B 726, 926 (2013)].
- [12] C. Krause, A. Pich, I. Rosell, J. Santos and J. J. Sanz-Cillero, JHEP **05**, 092 (2019), [1810.10544].
- [13] I. Brivio *et al.*, JHEP **03**, 024 (2014), [1311.1823].
- [14] I. Brivio and M. Trott, Phys. Rept. **793**, 1 (2019), [1706.08945].
- [15] LHC Higgs Cross Section Working Group, D. de Florian *et al.*, 1610.07922.
- [16] ATLAS, L. Barranco Navarro, PoS **LHCP2021**, 311 (2021).
- [17] ATLAS, CMS, A. Sciandra, PoS **LHCP2022**, 195 (2023).
- [18] ATLAS, CMS, E. Soldatov, PoS **LHCP2022**, 178 (2023).
- [19] O. J. P. Eboli, M. C. Gonzalez-Garcia and M. Martinez, Phys. Rev. D **105**, 053003 (2022), [2112.11468].
- [20] J. C. Criado, V. V. Khoze and M. Spannowsky, JHEP **12**, 026 (2021), [2109.01596].

- [21] T. Cohen, N. Craig, X. Lu and D. Sutherland, JHEP **12**, 003 (2021), [2108.03240].
- [22] I. n. Asiáin, D. Espriu and F. Mescia, Phys. Rev. D **105**, 015009 (2022), [2109.02673].
- [23] R. Alonso and M. West, Phys. Rev. D **105**, 096028 (2022), [2109.13290].
- [24] R. Gómez-Ambrosio, F. J. Llanes-Estrada, A. Salas-Bernárdez and J. J. Sanz-Cillero, Phys. Rev. D **106**, 053004 (2022), [2204.01763].
- [25] R. Gómez-Ambrosio, F. J. Llanes-Estrada, A. Salas-Bernárdez and J. J. Sanz-Cillero, 2207.09848.
- [26] M. J. Herrero and R. A. Morales, Phys. Rev. D **106**, 073008 (2022), [2208.05900].
- [27] D. Domenech, M. J. Herrero, R. A. Morales and M. Ramos, Phys. Rev. D **106**, 115027 (2022), [2208.05452].
- [28] A. Lindner and K. F. Muzakka, 2201.05122.
- [29] C. Quezada-Calonge, A. Dobado and J. J. Sanz-Cillero, Phys. Rev. D **107**, 093006 (2023), [2207.01458].
- [30] L. Gráf, B. Henning, X. Lu, T. Melia and H. Murayama, JHEP **02**, 064 (2023), [2211.06275].
- [31] H. Sun, Y.-N. Wang and J.-H. Yu, 2211.11598.
- [32] H. Sun, M.-L. Xiao and J.-H. Yu, JHEP **05**, 043 (2023), [2206.07722].
- [33] H. Sun, M.-L. Xiao and J.-H. Yu, JHEP **04**, 086 (2023), [2210.14939].
- [34] Z.-Y. Dong, T. Ma, J. Shu and Z.-Z. Zhou, JHEP **09**, 101 (2023), [2211.16515].
- [35] H. Liu, T. Ma, Y. Shadmi and M. Waterbury, JHEP **05**, 241 (2023), [2301.11349].
- [36] R. Alonso, 2307.14301.
- [37] I. n. Asiáin, D. Espriu and F. Mescia, Phys. Rev. D **108**, 055013 (2023), [2305.03622].
- [38] S. Dawson, D. Fontes, C. Quezada-Calonge and J. J. Sanz-Cillero, Phys. Rev. D **108**, 055034 (2023), [2305.07689].
- [39] F. Arco, D. Domenech, M. J. Herrero and R. A. Morales, Phys. Rev. D **108**, 095013 (2023), [2307.15693].
- [40] A. Bhardwaj, C. Englert, D. Gonçalves and A. Navarro, 2308.11722.
- [41] R. L. Delgado, R. Gómez-Ambrosio, J. Martínez-Martín, A. Salas-Bernárdez and J. J. Sanz-Cillero, 2311.04280.
- [42] O. J. P. Eboli, M. C. Gonzalez-Garcia and M. Martines, 2311.09300.
- [43] M. J. Herrero and R. A. Morales, Phys. Rev. D **104**, 075013 (2021), [2107.07890].

- [44] R. L. Delgado *et al.*, JHEP **11**, 098 (2017), [1707.04580].
- [45] ATLAS, G. Aad *et al.*, Phys. Rev. Lett. **113**, 141803 (2014), [1405.6241].
- [46] ATLAS, M. Aaboud *et al.*, Phys. Rev. D **95**, 032001 (2017), [1609.05122].
- [47] D. Espriu, F. Mescia and B. Yencho, Phys. Rev. D **88**, 055002 (2013), [1307.2400].
- [48] R. L. Delgado, A. Dobado and F. J. Llanes-Estrada, JHEP **02**, 121 (2014), [1311.5993].
- [49] R. L. Delgado, A. Dobado, M. J. Herrero and J. J. Sanz-Cillero, JHEP **07**, 149 (2014), [1404.2866].
- [50] G. Buchalla, O. Cata, A. Celis and C. Krause, Eur. Phys. J. C **76**, 233 (2016), [1511.00988].
- [51] M. Fabbrichesi, M. Pinamonti, A. Tonero and A. Urbano, Phys. Rev. D **93**, 015004 (2016), [1509.06378].
- [52] I. Brivio, J. Gonzalez-Fraile, M. C. Gonzalez-Garcia and L. Merlo, Eur. Phys. J. C **76**, 416 (2016), [1604.06801].
- [53] J. de Blas, O. Eberhardt and C. Krause, JHEP **07**, 048 (2018), [1803.00939].
- [54] ATLAS, ATL-PHYS-PUB-2022-019 (2022).
- [55] C. Grojean, O. Matsedonskyi and G. Panico, JHEP **10**, 160 (2013), [1306.4655].
- [56] R. Alonso, I. Brivio, B. Gavela, L. Merlo and S. Rigolin, JHEP **12**, 034 (2014), [1409.1589].
- [57] I. M. Hierro, L. Merlo and S. Rigolin, JHEP **04**, 016 (2016), [1510.07899].
- [58] M. B. Gavela, K. Kanshin, P. A. N. Machado and S. Saa, Eur. Phys. J. C **76**, 690 (2016), [1610.08083].
- [59] Y.-H. Qi, J.-H. Yu and S.-H. Zhu, Phys. Rev. D **103**, 015013 (2021), [1912.13058].
- [60] G. Buchalla, O. Cata, A. Celis and C. Krause, Nucl. Phys. B **917**, 209 (2017), [1608.03564].
- [61] S. Weinberg, Physica A **96**, 327 (1979).
- [62] A. Manohar and H. Georgi, Nucl. Phys. B **234**, 189 (1984).
- [63] E. E. Jenkins, A. V. Manohar and M. Trott, Phys. Lett. B **726**, 697 (2013), [1309.0819].
- [64] G. Buchalla, O. Catá and C. Krause, Phys. Lett. B **731**, 80 (2014), [1312.5624].
- [65] A. Pich, I. Rosell, J. Santos and J. J. Sanz-Cillero, JHEP **04**, 012 (2017), [1609.06659].
- [66] B. M. Gavela, E. E. Jenkins, A. V. Manohar and L. Merlo, Eur. Phys. J. C **76**, 485 (2016), [1601.07551].
- [67] S. Dittmaier, S. Schuhmacher and M. Stahlhofen, Eur. Phys. J. C **81**, 826 (2021), [2102.12020].
- [68] R. Alonso, E. E. Jenkins and A. V. Manohar, Phys. Lett. B **754**, 335 (2016), [1511.00724].

- [69] R. Alonso, E. E. Jenkins and A. V. Manohar, JHEP **08**, 101 (2016), [1605.03602].
- [70] B. Assi, A. Helset, A. V. Manohar, J. Pagès and C.-H. Shen, JHEP **11**, 201 (2023), [2307.03187].
- [71] M. Trott, EWPD in the SMEFT and the $\mathcal{O}(y_t^2, \lambda)$ one loop Z decay width, in *Proceedings, 52nd Rencontres de Moriond on Electroweak Interactions and Unified Theories: La Thuile, Italy, March 18-25, 2017*, pp. 63–70, 2017, [1705.05652].
- [72] T. Robens and T. Stefaniak, Eur. Phys. J. C **75**, 104 (2015), [1501.02234].
- [73] T. Robens and T. Stefaniak, Eur. Phys. J. C **76**, 268 (2016), [1601.07880].
- [74] S. Dawson, P. P. Giardino and S. Homiller, Phys. Rev. D **103**, 075016 (2021), [2102.02823].
- [75] A. Ilnicka, T. Robens and T. Stefaniak, Modern Physics Letters A **33**, 1830007 (2018).
- [76] D. López-Val and T. Robens, Physical Review D **90** (2014).
- [77] C. Englert *et al.*, J. Phys. G **41**, 113001 (2014), [1403.7191].
- [78] T. Robens, More Doublets and Singlets, in *56th Rencontres de Moriond on Electroweak Interactions and Unified Theories*, 2022, [2205.06295].
- [79] V. Barger, P. Langacker, M. McCaskey, M. Ramsey-Musolf and G. Shaughnessy, Phys. Rev. D **79**, 015018 (2009), [0811.0393].
- [80] R. Costa, M. Mühlleitner, M. O. P. Sampaio and R. Santos, JHEP **06**, 034 (2016), [1512.05355].
- [81] M. Mühlleitner, M. O. P. Sampaio, R. Santos and J. Wittbrodt, 1703.07750.
- [82] S. Dawson and M. Sullivan, Phys. Rev. D **97**, 015022 (2018), [1711.06683].
- [83] F. Egle, M. Mühlleitner, R. Santos and J. Viana, Physical Review D **106** (2022).
- [84] S. Adhikari, S. D. Lane, I. M. Lewis and M. Sullivan, Complex Scalar Singlet Model Benchmarks for Snowmass, in *Snowmass 2021*, 2022, [2203.07455].
- [85] F. Egle, M. Mühlleitner, R. Santos and J. a. Viana, 2306.04127.
- [86] T. D. Lee, Phys. Rev. **D8**, 1226 (1973).
- [87] J. F. Gunion, H. E. Haber, G. L. Kane and S. Dawson, Front. Phys. **80**, 1 (2000).
- [88] G. C. Branco *et al.*, Phys. Rept. **516**, 1 (2012), [1106.0034].
- [89] S. Dawson, D. Fontes, S. Homiller and M. Sullivan, Phys. Rev. D **106**, 055012 (2022), [2205.01561].
- [90] D. Fontes, M. Löschner, J. C. Romão and J. P. Silva, Eur. Phys. J. C **81**, 541 (2021), [2103.05002].
- [91] J. F. Donoghue and L. F. Li, Phys. Rev. D **19**, 945 (1979).
- [92] H. Georgi and D. V. Nanopoulos, Phys. Lett. B **82**, 95 (1979).

- [93] F. J. Botella and J. P. Silva, Phys. Rev. **D51**, 3870 (1995), [hep-ph/9411288].
- [94] G. C. Branco, L. Lavoura and J. P. Silva, Int. Ser. Monogr. Phys. **103**, 1 (1999).
- [95] D. Fontes, J. C. Romão and J. P. Silva, JHEP **12**, 043 (2014), [1408.2534].
- [96] Anisha, D. Azevedo, L. Biermann, C. Englert and M. Mühlleitner, 2311.06353.
- [97] J. Haller *et al.*, Eur. Phys. J. C **78**, 675 (2018), [1803.01853].
- [98] S. Kanemura, T. Kubota and E. Takasugi, Phys. Lett. **B313**, 155 (1993), [hep-ph/9303263].
- [99] A. G. Akeroyd, A. Arhrib and E.-M. Naimi, Phys. Lett. **B490**, 119 (2000), [hep-ph/0006035].
- [100] I. F. Ginzburg and I. P. Ivanov, Phys. Rev. D **72**, 115010 (2005), [hep-ph/0508020].
- [101] J. F. Gunion and H. E. Haber, Phys. Rev. D **67**, 075019 (2003), [hep-ph/0207010].
- [102] M. Carena, I. Low, N. R. Shah and C. E. M. Wagner, JHEP **04**, 015 (2014), [1310.2248].
- [103] D. Fontes and J. C. Romão, Comput. Phys. Commun. **256**, 107311 (2020), [1909.05876].
- [104] D. Fontes and J. C. Romão, JHEP **06**, 016 (2021), [2103.06281].
- [105] N. D. Christensen and C. Duhr, Comput. Phys. Commun. **180**, 1614 (2009), [0806.4194].
- [106] A. Alloul, N. D. Christensen, C. Degrande, C. Duhr and B. Fuks, Comput. Phys. Commun. **185**, 2250 (2014), [1310.1921].
- [107] P. Nogueira, J. Comput. Phys. **105**, 279 (1993).
- [108] R. Mertig, M. Bohm and A. Denner, Comput. Phys. Commun. **64**, 345 (1991).
- [109] V. Shtabovenko, R. Mertig and F. Orellana, Comput. Phys. Commun. **207**, 432 (2016), [1601.01167].
- [110] V. Shtabovenko, R. Mertig and F. Orellana, Comput. Phys. Commun. **256**, 107478 (2020), [2001.04407].
- [111] T. Hahn, Comput. Phys. Commun. **140**, 418 (2001), [hep-ph/0012260].
- [112] T. Hahn and M. Perez-Victoria, Comput. Phys. Commun. **118**, 153 (1999), [hep-ph/9807565].
- [113] A. Djouadi, V. Driesen, W. Hollik and A. Kraft, Eur. Phys. J. C **1**, 163 (1998), [hep-ph/9701342].
- [114] H. E. Haber *et al.*, Phys. Rev. D **63**, 055004 (2001), [hep-ph/0007006].
- [115] A. Arhrib, M. Capdequi Peyranere, W. Hollik and S. Penaranda, Phys. Lett. B **579**, 361 (2004), [hep-ph/0307391].
- [116] G. Bhattacharyya, D. Das, P. B. Pal and M. N. Rebelo, JHEP **10**, 081 (2013), [1308.4297].

- [117] P. M. Ferreira, J. F. Gunion, H. E. Haber and R. Santos, Phys. Rev. **D89**, 115003 (2014), [1403.4736].
- [118] D. Fontes, J. C. Romão and J. P. Silva, Phys. Rev. D **90**, 015021 (2014), [1406.6080].